Chromosome 8 gain drives poor patient outcome via expression of 4E-BP1 in Ewing sarcoma

Cornelius M. Funk[1,2], Martin F. Orth[3] Karim Aljakouch[4], Anna Ehlers[1,2], Jing Li[1,2], Tilman L. B. Hölting[1,2,5], Rainer Will[6], Franziska Willis[7], Endrit Vinca[1,2], Shunya Ohmura[1,2], Roland Imle[2,8,9,10], Maximilian M. L. Knott[11,12], Felina Zahnow[1,2], Ana Sastre[13], Javier Alonso[14,15], Felix Sahm[16,17], Martin Schneider[7], Ana Banito[2,8], Gabriel Leprivier[18], Wolfgang Hartmann[19], Uta Dirksen[20], Olaf Witt[2,21,22], Ina Oehme[2,22], Stefan M. Pfister[2,20,23], Laura Romero-Pérez[1,2, 24,25], Jeroen Krijgsveld[4], Florencia Cidre-Aranaz[1,2], Thomas G. P. Grünewald[1,2,3,26,*,§], Julian Musa[1,2,7,*]

* T.G.P.G. and J.M. share senior authorship

Author affiliations:
1 Division of Translational Pediatric Sarcoma Research (B410), German Cancer Research Center (DKFZ), Heidelberg, Germany
2 Hopp Children's Cancer Center Heidelberg (KiTZ), Heidelberg, Germany
3 Max-Eder Research Group for Pediatric Sarcoma Biology, Institute of Pathology, Faculty of Medicine, LMU Munich, Munich, Germany
4 Division of Proteomics of Stem Cells and Cancer, German Cancer Research Center (DKFZ), Heidelberg, Germany
5 Department of Medical Oncology, National Centre for Tumor Diseases, Heidelberg, Germany
6 Cellular Tools Core Facility, German Cancer Research Center (DKFZ), German Cancer Consortium (DKTK), Heidelberg, Germany
7 Department of General, Visceral and Transplantation Surgery, University Hospital Heidelberg, Heidelberg, Germany
8 Soft-Tissue Sarcoma Junior Research Group, German Cancer Research Center (DKFZ), Heidelberg, Germany
9 Division of Pediatric Surgery, University Hospital Heidelberg, Heidelberg, Germany
10 Faculty of Biosciences, Heidelberg University, Heidelberg, Germany
11 Institute of Pathology, Faculty of Medicine, LMU Munich, Munich, Germany
12 Department of Neurobiology, Faculty of Life Sciences & Sagol School of Neuroscience, Tel Aviv University, Tel Aviv, Israel
13 Unidad Hemato-oncología Pediátrica, Hospital Infantil Universitario La Paz, Madrid, Spain
14 Pediatric Solid Tumour Laboratory, Institute of Rare Diseases Research (IIER), Instituto de Salud Carlos III, Madrid, Spain
15 Centro de Investigación Biomédica en Red de Enfermedades Raras, Instituto de Salud Carlos III (CB06/07/1009; CIBERER-ISCIII), Madrid, Spain
16 Clinical Cooperation Unit Neuropathology (B300), German Cancer Consortium (DKTK), German Cancer Research Center (DKFZ), Heidelberg, Germany
17 Department of Neuropathology, University Hospital Heidelberg, Heidelberg, Germany
18 Institute of Neuropathology, University Hospital Düsseldorf, Medical Faculty, Heinrich Heine University, Düsseldorf, Germany
19 Division of Translational Pathology, Gerhard-Domagk-Institute of Pathology, University Hospital of Münster, Münster, Germany
20 Department of Pediatric Hematology and Oncology, University Hospital of Essen, Essen, Germany
21 Department of Pediatric Oncology, Hematology, Immunology and Pulmonology, Heidelberg University Hospital, Heidelberg, Germany
22 Clinical Cooperation Unit Pediatric Oncology, German Cancer Research Center (DKFZ) and German Consortium for Translational Cancer Research (DKTK), Heidelberg, Germany
23 Division of Pediatric Neurooncology, German Cancer Research Center (DKFZ) and German Consortium for Translational Cancer Research (DKTK), Heidelberg, Germany
24 Division of Molecular Pathology of Sarcomas, Institute of Biomedicine of Sevilla (IBiS), Virgen del Rocio University Hospital/CSIC/University of Sevilla/CIBERONC, Seville, Spain
25 Department of Normal and Pathological Cytology and Histology, School of Medicine, University of Seville, Seville, Spain
26 Institute of Pathology, Heidelberg University Hospital, Heidelberg, Germany

§ Address for correspondence
Thomas G. P. Grünewald, MD, PhD
Division Head, Division of Translational Pediatric Sarcoma Research (B410)
German Cancer Research Center (DKFZ) & Hopp-Children's Cancer Center (KiTZ)
Im Neuenheimer Feld 280, 69210 Heidelberg, Germany
Phone +49-6221-42-3718
Fax +49-6221-42-3721
Email t.gruenewald@kitz-heidelberg.de

Word count: 2646 (excluding Abstract, Materials & Methods, and Figure Legends)
Display items: 3 Figures, 3 Supplementary Figures, 9 Supplementary Tables
Running title: Chromosome 8 gain and EIF4EBP1 in Ewing sarcoma
Key words: Ewing sarcoma, chromosome 8 gain, EIF4EBP1, 4E-BP1

ABSTRACT

To refine patient care in the context of precision oncology, it is increasingly important to understand mechanisms underlying inter-individual tumor heterogeneity, especially in oligomutated cancers. Ewing sarcoma (EwS) is genetically characterized by pathognomonic *FET::ETS* gene fusions (in most cases *EWSR1::FLI1*) while featuring a general paucity of other recurrent somatic alterations that might account for observed diversity in clinical patient outcome. Following *FET::ETS* fusions, chromosome (chr) 8 gain is the second most common recurrent somatic alteration in EwS. However, its pathophysiological role and potential clinical implications remain unclear.

Here, we report that gene expression signatures indicative for chr8 gain are significantly associated with poor overall survival of EwS patients, and that this effect is predominantly mediated by expression of the translation initiation factor binding protein EIF4EBP1 (4E-BP1). High *EIF4EBP1* expression shows the strongest association with poor overall survival of EwS patients among all genes located on chr8, which as well holds true in a subgroup analysis of patients with localized disease, emphasizing the prognostic role of 4E-BP1 in EwS. Consistently, chr8 gain was associated with higher intra-tumoral *EIF4EBP1* expression in EwS patient samples. RNA interference-mediated knockdown of 4E-BP1 significantly decreased proliferation, clonogenicity, and spheroidal growth of EwS cells *in vitro* as well as tumor growth of EwS xenografts *in vivo*. To identify potential mechanisms via which 4E-BP1 mediates its phenotypic effect, we performed integrated proteomic and transcriptomic profiling of EwS cell lines with and without silencing of 4E-BP1 revealing that 4E-BP1 guides a multifunctional proteomic network including hubs associated with RNA processing, translational regulation, and chromatin modification.

Collectively, we establish a significant association between chr8 gain and unfavorable prognosis in EwS. We show that this association primarily depends on the expression of the translation initiation factor binding protein 4E-BP1 regulating a multifunctional proteomic network. Our data suggest that cytogenetic testing for chr8 gain in EwS tumors may help to improve risk-stratification of patients and adaptation of the therapeutic management.

INTRODUCTION

Ewing sarcoma (EwS) is a malignant bone- and soft tissue-related tumor, mainly occurring in children, adolescents, and young adults[1]. It is characterized by a low number of recurrent somatic mutations and driven by chromosomal translocations generating pathognomonic *FET::ETS* fusions (in 85% of cases *EWSR1::FLI1*) encoding aberrant chimeric transcription factors[1]. Genetic variants in polymorphic enhancer-like DNA binding sites of EWSR1::FLI1 were shown to account for inter-individual heterogeneity in EwS susceptibility, tumor growth, clinical course, and treatment response[2–4]. Although somatic mutations in *STAG2* and *TP53* occur in approximately 20 and 5% of patients[5–7], respectively, little is known about other, more common recurrent alterations such as chromosomal gains and/or losses regarding their impact on inter-individual tumor heterogeneity in EwS. However, understanding the mechanisms underlying inter-individual tumor heterogeneity and their effect on clinical courses in EwS is necessary to develop novel personalized diagnostic and therapeutic approaches.

Gain of chromosome (chr) 8 is found in approximately 50% of EwS cases, especially in form of chr8 trisomy, and thus constitutes the second most frequently observed recurrent somatic alteration in EwS following *FET::ETS* fusions[5–11]. So far, only few studies have addressed the role of chr8 gains in EwS[5–8,10,12–17], which is why their precise functional and clinical impact in EwS remains largely unexplored.

Therefore, the present study aimed at investigating the possible association between chr8 gains and EwS tumor progression and at identifying the clinically most relevant genes located on chr8 that may functionally contribute to inter-individual variability of EwS patient outcomes. Following an integrative functional genomics approach, we identify the eukaryotic translation initiation factor 4E binding protein 1 (EIF4EBP1, alias 4E-BP1), which acts downstream of its inactivating kinase complex mTORC1 (mammalian target of rapamycin complex 1) and is a main effector mTORC1 signaling pathway[18,19], as the most promising chr8 candidate gene being outstandingly associated with unfavorable patient outcome among all other captured genes located on chr8 and even across

the whole EwS transcriptome. 4E-BP1 belongs to a family of eIF4E-binding proteins via which mTORC1 essentially adapts mRNA translation rates to several stimuli by modulating the assembly of the 48S translation pre-initiation complex, and whose role in tumor initiation/progression is not yet definitive[18]. We show that overexpression of *EIF4EBP1* is mediated by chr8 gain in primary EwS tumors, and that its RNAi-mediated knockdown in cell line models reduces EwS growth *in vitro* and *in vivo* by guiding a multifunctional proteomic network, thus establishing an association between chr8 gain and tumor progression mediated by 4E-BP1 in EwS.

RESULTS

Chromosome 8 gain drives overexpression of the clinically relevant translation initiation factor 4E-BP1 in EwS

To obtain first insights into the potential role of chr8 gain as a mediator of poor patient outcome in EwS, we analyzed a cohort of 196 EwS samples for which matched microarray gene expression data and clinical data were available (henceforth referred to as 'Cohort 1'). From gene expression data, we inferred chr8 gene enrichment using a chr8 gene signature and performed a single-sample Gene Set Enrichment Analysis (ssGSEA) followed by hierarchical clustering (k=2) assigning each patient into either a high or low chr8 gene expression signature group (**Figure 1a**). To validate appropriate clustering of tumor samples, we determined differentially expressed genes (DEGs) between the chr8 high and low gene expression signature cluster and performed a Position Related Data Analysis (PREDA) to map respective DEGs to chromosomal positions, showing that DEGs preferentially map to chr8 (**Supplementary Figure 1a**). Interestingly, within genes of the mTOR signaling pathway, 4E-BP1 seems to be distinctively differentially upregulated in EwS belonging to the chr8 high gene expression signature group (**Supplementary Figure 1b**). Kaplan-Meier analysis revealed that high chr8 gene expression signature was associated with shorter overall EwS patient survival (P=0.0137, **Figure 1b**). Strikingly, even when only considering patients with localized disease (i.e. without evidence for metastasis at diagnosis), this association still remained significant (P=0.0309,

Figure 1b), indicating that chr8 gain might be functionally involved in mediating an unfavorable disease phenotype. In support of this hypothesis, it is intriguing that while chr8 gain is found only in approximately 50% of primary tumors, around 78% of EwS cell lines exhibit chr8 gains (mostly trisomies)[5–8,10,13–17]. Together, these findings suggest that genes located on chr8 contribute to aggressive cellular behavior and disease progression in EwS.

To identify genes located on chr8 that are strongly associated with overall survival of EwS patients, we performed a batch-analysis within Cohort 1 calculating *P*-values for the association with overall patient survival for every gene represented on the microarray using the custom code software GenEx applying Mantel-Haenszel statistics (**Supplementary Table 1**). Of those covered genes located on chr8, high expression of *EIF4EBP1* stood out due to the strongest association with overall survival (**Figure 1c**, **Supplementary Table 2**). Additionally, *EIF4EBP1* ranked within the top 15 survival associated genes genome-wide (**Figure 1c, Supplementary Table 1**). Indeed, high expression of *EIF4EBP1* correlated highly significantly (nominal $P<0.0001$, Bonferroni-adjusted $P=0.049$, **Figure 1d**) with worse overall survival of EwS patients. Notably, in consistence with the association of chr8 gain with poor overall survival, high *EIF4EBP1* expression also remained significantly associated with poor patient overall survival even when only considering patients with localized disease ($P=0.0013$, **Figure 1d**).

To verify the association between chr8 gain and *EIF4EBP1* expression in an independent cohort, we analyzed genome-wide copy-number variation (CNV) data (inferred from DNA methylation arrays) of 99 EwS tumors for which matched gene expression data from RNA-sequencing were available (henceforth referred to as 'Cohort 2'). The results showed that gain of chr8 is significantly associated with higher *EIF4EBP1* expression ($P<0.001$; **Figure 1e**).

Collectively, these results indicate that chr8 gain might mediate unfavorable EwS patient outcome and highlighted 4E-BP1 as a potential driver of EwS aggressiveness encoded on chr8.

4E-BP1 promotes EwS tumorigenicity *in vitro* and *in vivo*

In contrast to our findings that high *EIF4EBP1* levels significantly correlated with worse patient outcome (**Figures 1c–d**), and despite the role of 4E-BP1 in cancer being complex, strongly depending on the cellular context and its precise phosphorylation status[18], a recent report has suggested that 4E-BP1 may act as a tumor suppressor in EwS[20]. However, this conclusion was based on observations upon supraphysiological, ectopic overexpression of a phospho-mutant (and thus functionally inactive) 4E-BP1 protein in two EwS cell lines (EW8 and TC-71)[20]. To obtain a potentially more accurate view on 4E-BP1 in EwS and to generate first functional insights regarding its *in situ* role, we performed two pre-ranked fast Gene Set Enrichment Analyses (fGSEA) using gene expression data from Cohorts 1 and 2 by calculating Pearson´s correlation coefficients between the mRNA expression levels of *EIF4EBP1* and those of every other gene represented in the respective dataset (**Supplementary Table 3–4**). Additionally, we carried out a third fGSEA using Cohort 1 by calculating the fold-changes (FCs) of all captured genes between tumors with and without predicted global chr8 gain (**Supplementary Table 5**). As an overlap between all three analyses, predominantly proliferation-associated gene sets were significantly enriched with predicted chr8 gain and *EIF4EBP1* expression at the mRNA level (**Figure 2a–b, Supplementary Table 3–4**). These transcriptomic data pointed toward a role of 4E-BP1 in the regulation of EwS cell proliferation and supported the potential role of 4E-BP1 as a major mediator of chr8 gain-mediated poor prognosis in EwS.

To further explore this hypothesis, we carried out functional experiments in EwS cell lines with relatively high *EIF4EBP1* expression levels (A-673, SK-N-MC, and TC-71) (**Supplementary Figure 2a**), two of which (SK-N-MC and TC-71) exhibit a chr8 gain[15]. To that end, we transduced EwS cell lines with a lentivirus containing a vector-system (pLKO Tet-on) with doxycycline (Dox)-inducible shRNAs, specifically directed against *EIF4EBP1* (sh4E-BP1_1 or sh4E-BP1_2) or a non-targeting control shRNA (shCtr). Both targeted shRNAs efficiently silenced 4E-BP1 expression as revealed by qRT-PCR and western blotting (**Supplementary Figure 2b–d**).

Since *EIF4EBP1* expression levels appeared to correlate with pro-proliferative signatures in EwS tumors (**Figure 2a–b**), we carried out proliferation assays. Knockdown of 4E-BP1 for 96h significantly inhibited cell proliferation in all three cell lines (**Figure 2c**). This anti-proliferative effect of 4E-BP1 knockdown appeared to be independent from cell death as Trypan-Blue-exclusion assays did not show a consistent significant effect of 4E-BP1 knockdown on cell death across all cell lines and shRNAs (**Supplementary Figure 2e**). In agreement with these short-term assays, prolonged 4E-BP1 knockdown (10–14d) significantly reduced both 3D anchorage-independent and 2D clonogenic growth of EwS cells (**Figure 2d–e**). Such effects were not observed in shControl cells (**Figure 2d–e**). Similarly, knockdown of 4E-BP1 significantly reduced growth of A-673 and TC-71 EwS cells subcutaneously xenotransplanted in flanks of NSG mice (**Figure 2f**, **Supplementary Figure 2f**). This phenotype was associated with a significantly diminished mitotic cell count as revealed by histologic assessment of the respective xenografts (**Figure 2g, Supplementary Figure 2g**), whereas no difference in tumor necrosis was observed between xenografts with and without 4E-BP1 knockdown (**Supplementary Figure 2h–i**). To further evaluate the effect observed in subcutaneous EwS xenografts in an orthotopic xenograft model, TC-71 cells transduced with an inducible *EIF4EBP1* targeting shRNA construct (sh4E-BP1_2) were xenografted into the proximal tibia of NSG mice, which were subsequently treated with or without Dox. In accordance with our subcutaneous xenograft model, tumor burden in orthotopic EwS xenografts was decreased upon Dox-induced knockdown of 4E-BP1 (**Supplementary Figure 2j**). In synopsis with our findings from our patient data (**Figures 1b–d**), these functional preclinical data provide strong evidence that high 4E-BP1 expression promotes rather than suppresses EwS growth.

4E-BP1 guides a multifunctional proteomic network

As 4E-BP1 is a regulator of mRNA translation initiation, which binds to the translation initiation factor eIF4E and thereby modifies overall and selective translation rates[18], we performed proteomic profiling of newly synthesized proteins to obtain mechanistic insights on how 4E-BP1 mediates its

phenotype. We employed mass spectrometry (MassSpec) to analyze the proteome of A-673, SK-N-MC, and TC-71 EwS cells with and without Dox-inducible shRNA-mediated knockdown of 4E-BP1 for 96h (using respective cell lines with either two different specific shRNAs targeting *EIF4EBP1* or a non-targeting negative control shRNA), which were pulsed with SILAC media and the methionine analog L-Azidohomoalanine (AHA) for 6h. To additionally identify proteins that may be indirectly regulated by 4E-BP1, i.e. at the transcriptional level, we paralleled our proteomic read-outs with transcriptome profiling of the same cells using gene expression microarrays. Depending on the cell line, our MassSpec analyses captured 4,800–7,000 proteins. Those proteins, which were only detected in one of the cell lines and those whose log2FCs showed a standard deviation ≥0.5 between cell lines (empirically chosen cut-off), were not considered for further analyses, yielding 5,905 remaining proteins. Our microarray experiments captured 11,300 genes across all three cell lines. Following empirically chosen cut-offs, genes whose log2FCs showed a standard deviation ≥0.5 between cell lines, were not considered for further analyses (8,726 remaining genes). Proteins were only considered as being directly regulated by 4E-BP1 when their mRNA log2 FCs were <|0.4| (3,864 proteins remaining).

After identification of differentially expressed proteins upon 4E-BP1 knockdown, which were not regulated by 4E-BP1 at the mRNA level across all three cell lines and both targeted shRNAs, (**Supplementary Table 6**), a pre-ranked fGSEA and weighted correlation gene network analysis (WCGNA) were performed for C2 and C5 collections of gene sets from the Molecular Signatures Database (MSigDB). The WCGNA revealed multiple key hubs of 4E-BP1-regulated protein sets comprising a broad functional spectrum such as translational regulation, RNA processing, and chromatin modification (**Figure 3a–b, Supplementary Table 7**). As our results from transcriptomic fGSEAs of primary EwS (**Figure 2 a–b**, **Supplementary Table 3–4**) and our functional data in EwS cell lines (**Figure 2c–g**) indicate a role of 4E-BP1 in mediating altered proliferation of EwS cells, the data from WCGNA of directly 4E-BP1-regulated proteins suggest that 4E-BP1 modulates

a variety of functional pathways to control this observed phenotype (**Figure 3a–b, Supplementary Table 7**).

While these findings warrant further investigation, our results indicate that 4E-BP1 regulates a multifunctional proteomic network that may mediate its observed phenotype in EwS.

DISCUSSION

The herein presented data establishes chr8 gain, the second most common somatic alteration in EwS, as an unfavorable prognostic factor in EwS, which is likely mediated to a great extent via overexpression of the translation initiation factor 4E-BP1 guiding multifunctional proteomic signatures.

In precision oncology, it is increasingly important to decipher mechanisms underlying inter-tumoral heterogeneity to refine diagnostic and therapeutic algorithms[3,21,22]. In this context, the identification of chr8 gain as a prognostic factor in EwS emphasizes the relevance of cytogenetic testing, which may help stratify patients into prognostic and/or therapeutic subgroups. Although chr8 trisomies are observed in approximately 50% of EwS patients, so far only trends or moderate associations of whole chr8 gain (i.e. trisomies) and poor patient outcome were observed[10,12–14,23–25]. Our data provide evidence for a significant association between a high chr8 gene expression signature and poor overall survival of EwS patients (**Figure 1b**). As this association remains statistically significant even when only considering patients with localized disease (**Figure 1b**), chr8 gain as assessed by cytogenetic testing or fluorescence in situ hybridization (FISH) or a high chr8 gene expression signature score (i.e., as assessed by ssGSEA) might serve as a prognostic biomarker for poor overall patient survival and thus might specifically help to stratify patients with localized disease into different treatment groups.

Interestingly, partial chr8 gain is observed in 48–78% of EwS family tumors and specifically gain of chr8p, where *EIF4EBP1* is located, was shown to be associated with EwS relapse[23,26]. Functionally, as *MYC* is located on chr8, the expression of MYC has been suspected to mediate a

potential effect of chr8 gain on EwS patient outcome[23,27]. However, expression of *MYC* was not significantly associated with overall EwS patient survival in our cohort of 196 primary EwS with matched clinical annotations (*P*=0.689, **Supplementary Table 1**, **Supplementary Figure 3a–b**), suggesting that mechanisms underlying the association of chr8 gain with EwS aggressiveness is more complex than previously anticipated. In line with this notion, recent evidence has indicated that chr8 gain mitigates EWSR1::FLI1-induced replication stress via expression of RAD21 resulting in promotion of EwS tumorigenicity[12]. Still, high expression of *RAD21* did not reach a significant association with overall EwS patient survival in our cohort (*P*=0.174; **Supplementary Table 1**).

Our results are in line with data from other cancer entities showing a prognostic/predictive value of chr8 gain, as for instance in acute myeloid leukemia[28] and chronic myeloid leukemia[29,30]. Interestingly, chr8 gain occurs in several other sarcoma entities, such as myxoid liposarcoma[31], clear cell sarcoma[32], and pediatric undifferentiated sarcomas[27]. Also, specifically amplification of the *EIF4EBP1* locus has been described in several other cancer entities[33]. Nonetheless, the prognostic value of chr8 gain in the latter entities remains unclear. Also, other possible mechanisms of *EIF4EBP1* upregulation except for chr8 gains across cancer entities have been described, as for example differential upregulation by other transcription factors[3,34], but in general require further investigation.

Moreover, recent data suggest that expression of non-phosphorylated 4E-BP1 may has a more oncogenic role by promoting cell survival in the context of nutrient starvation of a cell[35]. As throughout the literature oncogenic and tumor suppressive roles of 4E-BP1 are described and as the phosphorylation status seems to impact its functional role[18], ongoing research in our laboratory aims at investigating the mechanistic/translational impact of the expression level ratio of phospho-4E-BP1 to total-4E-BP1, as well as at the identification of differential drug sensitivity of 4E-BP1 high expressing tumors in order to specifically treat such tumors in the context of personalized cancer therapy.

In sum, our data suggest that chr8 gain has an important prognostic role in EwS and that its functional effects on tumor progression are mainly driven by increased 4E-BP1 expression. As chr8 gain occurs in approximately 50% of EwS cases, our results indicate this chromosomal aberration to be a major source of inter-tumoral heterogeneity in EwS and that further cytogenetic testing of EwS might offer a refinement of clinical management in the context of precision oncology.

MATERIALS AND METHODS

Provenience of cell lines and cell culture conditions

Human EwS cell line A-673 (RRID:CVCL 0080) and human HEK293T cells (RRID:CVCL_0063) were purchased from American Type Culture Collection (ATCC). Human EwS cell line SK-N-MC (RRID:CVCL 0530) was provided by the German collection of Microorganisms and Cell cultures (DSMZ). Human EwS cell line TC-71 (RRID_CVCL_2213) was provided by the Children's Oncology Group (COG). All cell lines were grown at 37 °C and 5% CO_2 in humidified atmosphere in RPMI 1640 medium supplemented with stable glutamine (Biochrom), 10% tetracycline-free fetal calf serum (FCS) (Sigma-Aldrich), 100 U/ml penicillin (Biochrom), and 100 µg/ml streptomycin (Biochrom) was used to grow the cells. Cells were routinely checked by nested PCR for mycoplasma infection. Cell line purity and authenticity was confirmed by STR-profiling.

Nucleotide extraction, reverse transcription, and quantitative real-time PCR (qRT-PCR)

Genomic DNA from human cell lines was extracted with the NucleoSpin Tissue kit (Macherey-Nagel), plasmid DNA was extracted from bacteria with the PureYield kit (Promega). RNA was extracted with the NucleoSpin II kit (Macherey-Nagel) and reverse-transcribed using the High-Capacity cDNA Reverse Transcription kit (Applied Biosystems). qRT-PCR reactions were performed using SYBR green Mastermix (Applied Biosystems) mixed with diluted cDNA (1:10) and 0.5 μM forward and reverse primer (total reaction volume 15 μl) on a BioRad Opus instrument and analyzed using BioRad CFX Manager 3.1 software. Gene expression values were calculated

using the $2^{-(\Delta\Delta Ct)}$ method[36] relative to the housekeeping gene *RPLP0* as internal control. Oligonucleotides were purchased from MWG Eurofins Genomics and are listed in **Supplementary Table 8.** The thermal conditions for qRT-PCR were as follows: initialization (95 °C, 2 min) (1 cycle); denaturation (95 °C, 10 sec), annealing (60 °C, 10 sec), and extension (60 °C, 10 sec) (49 cycles); denaturation (95 °C, 30 sec), annealing (65 °C, 30 sec), extension (melting curve 65 °C increasing 0.5 °C every 5 sec until 95 °C) (1 cycle).

Generation of doxycycline (Dox)-inducible shRNA constructs

Human EwS cell lines A-673, SK-N-MC, and TC-71 were transduced with lentiviral Tet-pLKO-puro all-in-one vector system (plasmid #21915, Addgene) containing a puromycin-resistance cassette, and a tet-responsive element for Dox-inducible expression of shRNAs against *EIF4EBP1* (sh4E-BP1_1 or sh4E-BP1_2) or a non-targeting control shRNA (shCtr). Sequences of the used shRNAs are listed in **Supplementary Table 8**. Dox-inducible vectors were generated according to a publicly available protocol[37] using In-Fusion HD Cloning Kit (Clontech). Vectors were amplified in Stellar Competent Cells (Clontech) and respective integrated shRNA was verified by Sanger sequencing. The used sequencing primer is listed in **Supplementary Table 8**. Lentiviral particles were generated in HEK293T cells. Virus-containing supernatant was collected to infect the human EwS cell lines. Successfully transduced cells were selected with 1.5 μg/ml puromycin (InVivoGen). The shRNA expression for *EIF4EBP1* knockdown or expression of a negative control shRNA in EwS cells was achieved by adding 0.5 μg/ml Dox every 48 h to the medium. Generated cell lines were designated as A-673/TR/shCtr, A-673/TR/sh4E-BP1_1, A-673/TR/sh4E-BP1_2, SK-N-MC/TR/shCtr, SK-N-MC/TR/sh4E-BP1_1, SK-N-MC/TR/sh4E-BP1_2, TC-71/TR/shCtr, TC-71/TR/sh4E-BP1_1, and TC-71/TR/sh4E-BP1_2.

Western blot

A-673, TC-71, and SK-N-MC cells were treated for 96h with Dox to induce *EIF4EBP1* knockdown.

Whole cellular protein was extracted with RIPA buffer (Serva electrophoresis) containing protease inhibitor cocktail and phosphatase inhibitor cocktail (Roche). Western blots were performed following routine protocols[38], and specific band detection was achieved by the use of rabbit monoclonal anti-4E-BP1 (clone Y329, 1:2,000, ab32024, Abcam) and rabbit polyclonal anti-p-4E-BP1 antibody (1:1,000, Ser65, #9451, Cell Signaling) and mouse monoclonal anti-ß-actin (1:5,000, A-5441, Sigma-Aldrich). Anti-rabbit IgG horseradish peroxidase coupled antibody (1:2,000, sc-516102, Santa Cruz Biotechnology) and anti-mouse IgG horseradish peroxidase coupled antibody (1:2,000, sc-2357, Santa Cruz Biotechnology) were used as secondary antibodies.

Proliferation assays

Depending on the cell line, 30–70 × 10^3 cells containing either a Dox-inducible non-targeting control shRNA or *EIF4EBP1*-targeting specific shRNAs were seeded in triplicate wells of a 6-well plate in 2 ml of growth medium. The cells were treated either with or without Dox (0.5 µg/ml; Sigma-Aldrich) for 120 h (medium was changed after 72 h including fresh Dox). Afterwards, cells of each treatment condition were harvested (including supernatant), stained with Trypan blue (Sigma-Aldrich), and viable as well as dead cells were counted in a standardized hemocytometer (C-chip, NanoEnTek). The assays were performed according to routine protocols[39].

Clonogenic growth assays (Colony forming assays)

Depending on the cell line, 500–1,000 cells containing either a Dox-inducible non-targeting control shRNA or *EIF4EBP1*-targeting specific shRNAs were seeded in triplicate wells of a 12-well plate in 2 ml of growth medium. Cells were grown with or without Dox (0.5 µg/ml) for 8–14 d depending on the cell line and afterwards stained with crystal violet (Sigma-Aldrich). Colony number and area was determined on scanned plates using Fiji (Image J)[40,41]. Clonogenicity index was calculated by multiplying the counted colonies with the corresponding colony volume.

Spheroidal growth assays

Depending on the cell line, 1,500–4,000 cells containing either a Dox-inducible non-targeting control shRNA or *EIF4EBP1*-targeting specific shRNAs were seeded in Costar Ultra-low attachment plates (Corning) for 8–14 d in 150 µl growth medium. To maintain the 4E-BP1 knockdown, 10 µl of fresh medium with or without Dox was added every 48 h to the cells. At day 8–14, the wells were photographed and spheres larger than 500 µm in diameter were counted. The area was measured using ImageJ. The sphere volumes were calculated as follows: $V = 4/3 \times \pi \times r^3$. The sphere index was calculated by multiplying the counted colonies with the corresponding colony volume.

Mass spectrometry (MassSpec)

Pulse-Chase Labelling using AHA (azidohomoalanine) and SILAC isotope labels for nascent proteome analysis: A-673, SK-N-MC, and TC-71 EwS cells containing either a Dox-inducible non-targeting control shRNA or *EIF4EBP1*-targeting specific shRNAs (sh_4E-BP1_1 or sh_4E-BP1_2) were seeded at a density of 1×10^6 per 15-cm dish in 20 ml of culture medium and grown with or without Dox (0.5 µg/ml; Sigma-Aldrich) for 96h. Subsequently, cells were washed with pre-warmed PBS and cultivated in 10 ml SILAC RPMI deprivation media (lysine-, arginine-, and methionine-free) (Athenas) for 45 min at 37°C. This ensures the depletion of the intracellular stores of amino acid. The depletion medium was then aspirated and cells were incubated in 13 ml of SILAC RPMI pulse media containing 18.1 mg/l AHA (Jena Bioscience), and either 200 mg/l [13C6, 15N4] L-arginine and 40 mg/l [13C6, 15N2] L-lysine or 200mg/l [13C6] L-arginine and 40 mg/l [4,4,5,5-D4] L-lysine (Silantes) for 6h at 37°C with 5% CO_2. Following pulse labelling, cells were washed with PBS and harvested by scraping and centrifugation for 5 min at 400× g. Cell pellets were frozen and stored at –80°C until lysis. Enrichment of newly synthesized proteins for translatome analysis and sample preparation for LC-MS/MS measurements: Newly synthesized proteins were enriched using the Click-It alkyne agarose enrichment kit (Thermo Fisher) according to the manufacturer protocol

with minor modifications. Cell pellets were lysed in 900 µl of Urea Lysis buffer (200 mM HEPES pH8, 0.5 M NaCl, 4% CHAPS, 8 M Urea), and cell lysates were sonicated on ice using the Benson probe sonicator. Protein concentrations were determined using the BSA kit (Thermo Fisher) and 1 mg of each label pair (+/– Dox) were mixed in a new tube. Volumes were made up to 1,700 µl end volume with 8M Urea lysis buffer. Next, the mixed lysates were combined with 100 µl of the alkyne-agarose slurry and 93 µl of the [3+2] cyclo-addition reaction mixture (10 µl Cu(II)SO4 (200 mM), 62.5 µl tris (hydroxypropyltriazolylmethyl) amine (THPTA, 160 mM), 10 µl aminoguanidine (2 M), 10 µl sodium ascorbate (2 M)), and incubated on a ThermoMixer for 2 h at 40°C. Following the incubation step, the resins were pelleted by centrifugation for 1 min at 2,000× *g* and supernatants were discarded. Subsequently, the resins were washed once with 2 ml of MQ water and pelleted by another centrifugation step. Next, the resins were resuspended in 2 ml of the 1-step reduction/alkylation mixture (10 mM Tris(2-carboxyethyl)phosphine, 40 mM 2-Chloroacetamide in SDS wash buffer) and incubated on a ThermoMixer for 15 min at 70 °C and another 15 min at 20 °C. Following the reduction/alkylation step, the resins were transferred into spin columns (BioRad) and placed on a P10 tip-box for the subsequent steps. The resins were consecutively washed five times with 1 ml SDS-Wash buffer (100 mM Tris-HCl pH 8.0, 1% SDS, 250 mM NaCl, 5 mM EDTA), once with MQ water, five times with Guanidine-Wash buffer (100 mM Tris-HCl pH 8.0, 6M Guanidine-HCl), and 5× with Acetonitrile-Wash buffer (20% Acetonitrile, ULCMS in Water ULCMS). Subsequently, the resins were resuspended in 200 µl Digestion buffer (100 mM Tris-HCl pH 8, 2 mM CaCl2, 5% Acetonitrile), transferred to new tubes, and subjected to proteolytic digestion by adding 1 µg of trypsin on a ThermoMixer for 16h at 37 °C. Following the digestion step, the resins were pelleted by centrifugation for 5 min at 2,000× g, the supernatants containing the digested peptides were transferred to new tubes and acidified with formic acid (FA) to 1% end concentration. For the peptide clean-up step, Oasis PRiME HLB µElution Plates (Waters) were used according to the manufacturer protocol. Briefly, the digested peptides were transferred to the Oasis plate and washed consecutively with 750 µl, 250 µl, and 100 µl of 1% FA. Peptides were eluted in a 96-well

plate by adding 70 µl of elution solution (60% MeOH, 1% FA, 39% Water ULCMS) and another 50 µl of 100% MeOH. The eluted peptides were then dried down using a SpeedVac, resuspended in 0.1% TFA, and samples were subjected to HPLC fractionation and mass spectrometry analysis. LC-MS/MS analysis: Samples were analyzed on an Orbitrap Fusion mass spectrometer (Thermo Fisher) coupled with an Easy-nLC 1200 system (Thermo Fisher). Chromatographic separation was carried out using an Acclaim Pepmap RSLC trap column (100 µm × 2 cm, 5 µm particles, 100 Å pores, C18, Thermo Fisher), and nanoEase M/Z Peptide BEH analytical column, (75 µm × 250 mm, 1.7 µm particles, 130Å pores, C18, Waters). Peptides elution gradient was set to 105 min at flow rate of 300 nl/min using solvent A (0.1% formic acid in ULCM grade water) and solvent B (0.1% formic acid in 80% acetonitrile and 19.9% ULCM grade water). Samples were injected into the mass spectrometer using a 10 µm Picotip coated fused silica emitter (New Objective). The Orbitrap-Fusion mass spectrometer was operating in positive mode. Acquisition was carried out in data-dependent acquisition (DDA) mode. The MS1 scan was detected in orbitrap mode at 60,000 FWHM resolution, AGC target 1E6, scan range (m/z) was 375–1,500 DA, and maximal injection time was set to 50 ms. The intensity threshold HCD-fragmentation was set to 5E3. MS2 detection was acquired in centroid mode with an HCD collision energy of 33% in an ion trap detector, an isolation window (m/z) of 1.6 Da, AGC target 1E4, and maximal injection time of 50 ms. Data analysis: The raw files were analyzed using MaxQuant (version 1.6.10.43). The MS/MS spectra were searched through the integrated Andromeda search engine against Homo Sapiens UniProt proteome database. Multiplicity of labels was set to 3. Arg6/Lys4 and Arg10/Lys8 were selected as medium and heavy labels, respectively. Cysteine carbamidomethylation was selected for fixed modification. Methionine oxidation, protein N-terminal acetylation, replacement of methionine by AHA and conversion of AHA to homoserine (HS) and diaminobutyrate (DAB) were selected for variable modifications. Re-quantify and match between runs (match time window: 0.4 min) functions were enabled. For the digestion, Trypsin/P was selected, and the maximal number of mis-cleavages was set to 2. The minimal peptide length was set to 7 amino acids and FDR for peptide and protein

identification was set to 0.01. For protein identification, at least one unique peptide was required. Minimum ratio count for label-based protein quantification was set to 2. Normalized H/M ratios derived from the ProteinGroups file were further processed and subjected to statistical analysis. FDR was set to >0.05 and S0 to 0.1. MassSpec profiling was performed in biological triplicates for every cell line/construct/condition. For analysis of differential protein expression, log2 fold changes (log2FCs) between conditions with and without Dox treatment were calculated for every cell line, every construct, and every biological replicate. A mean log2FC across biological replicates was calculated for every cell line/construct and the mean log2FCs of both used specific shRNAs (sh_4E-BP1_1 and sh_4E-BP1_2) were summarized and normalized to that of the shCtr. Normalized log2 fold changes were summarized across cell lines. Proteins which were only detected in one of the cell lines and proteins whose log2FCs showed a standard deviation ≥0.5 between cell lines were not considered for further analyses. Proteins were only considered as being directly regulated by 4E-BP1 in case that their log2FCs at the mRNA level according to microarray profiling were within a log2FC between –0.4 and 0.4, implying that they are not regulated on mRNA level in a relevant manner. Cut-offs were chosen empirically.

Xenotransplantation experiments

To assess local tumor growth of subcutaneous xenografts *in vivo*, 2.5×10^6 A-673 or TC-71 EwS cells containing either a Dox-inducible negative control shRNA or specific shRNAs against *EIF4EBP1* were injected subcutaneously with a 1:1 mix of PBS (Biochrom) and Geltrex (LDEV-Free Reduced Growth Factor Basement Membrane Matrix, Thermo Fisher Scientific; max volume 100 µl) in the right flanks of 4–8 week old NSG mice (Charles River Laboratories) following routine protocols[42]. When tumors were first palpable, mice were randomized to the control group (17.5 mg/ml sucrose (Sigma-Aldrich) in drinking water) or the treatment group (2 mg/ml Dox (Beladox, bela-pharm) and 50 mg/ml sucrose (Sigma-Aldrich) in drinking water). According to the average water intake of mice in the different treatment groups, the concentration of sucrose in the different

treatment groups has been adapted: due to the bitter tase of Dox, the mice that receive Dox via their drinking water in average have a lower water intake, making a higher concentration of sucrose necessary to ensure equal intake of sucrose per mouse across the different treatment groups. Tumor size was measured with a caliper every two days and tumor volume was calculated as $V=a\times b^2/2$ with a being the largest diameter and b the smallest. Once tumors reached size maximum of 15 mm in one dimension (event), respective mice were sacrificed by cervical dislocation. Other specific humane endpoints were determined as follows: invasive tumor growth leading to functional impairment or pain, ulcerating tumor (or fluid externalization), prolonged obstipation, abdominal distention, peritonitis, ascites, bloody diarrhea, palpable abdominal tumor mass with additional signs of pain, total relief, or medium paresis of a limb. General humane endpoints were determined as follows: Loss of 20% body weight, apathy, piloerection, self-isolation, aggressivity, automutilation, unphysiological or reduced movements/positioning, abnormal breathing, and reaching of a maximum observation period of 12 months.

For analysis of EwS xenograft growth in bone, TC-71/TR/sh4E-BP1_2 EwS cells were orthotopically injected into the proximal tibial plateau of NSG mice. One day before injection, mice were pre-treated with 800 mg/kg mouse weight/d Metamizole in drinking water as analgesia. On the day of injection, mice were anesthetized with inhaled isoflurane (2.5% in volume) and their eyes were protected with Bepanthen eye cream. After disinfection of the injection site, 2×10^5 cells/20 µl were directly injected with a fine 30 G needle (Hamilton) into the right proximal tibia. For pain prophylaxis until the first day after intraosseous injection, mice were treated with Metamizole in drinking water (800 mg/kg mouse weight/d). The first day after injection of tumor cells, mice were randomized in two groups of which one received henceforth 2 mg/ml Dox (BelaDox, Bela-pharm) dissolved in drinking water containing 5% sucrose (Sigma-Aldrich) to induce sh4E-BP1_2 expression, whereas the other group only received 5% sucrose. All tumor-bearing mice were sacrificed by cervical dislocation when the mice exhibited limping at the injected leg (event) or reached any humane endpoint as listed above.

Animal experiments were approved by the government of Upper Bavaria and North Baden and conducted in accordance with ARRIVE guidelines, recommendations of the European Community (86/609/EEC), and United Kingdom Coordinating Committee on Cancer Research (UKCCCR) guidelines for the welfare and use of animals in cancer research.

Methylation arrays and CNV analysis of primary EwS samples

A minimum of 500 ng of high-quality DNA from 99 EwS FFPE samples was used for methylation and CNV analysis with the Infinium Human Methylation 450K BeadChip (EPIC array; Illumina). This method can analyze 864,928 CpGs including main CpG islands and CpG sites outside of CpG islands. Raw methylation and CNV data were essentially processed as previously reported[43]. Based on the methylome, we used a previously described sarcoma classifier[43], which assigns a score to each sample indicating the similarity of the respective methylome with methylation patterns of samples from known entities. CNVs were also assessed by this method and analyzed at both, chromosomal and specific locus level. Scores for specific positions were visualized in the Integrative Genomic Viewer (IGV).

For analysis regarding the association between chr8 gain and *EIF4EBP1* expression (as assessed by RNA-seq), only samples were analyzed which were clearly possible to separate into either a group showing global chr8 gain or no chr8 gain. Samples with partial gain were not considered.

RNA sequencing (RNA-seq)

RNA quality was assessed by the Agilent 2100 Bioanalyzer (Agilent Technologies) before library preparation. 2 µg of estimated high-quality RNA were prepared for sequencing. Libraries were prepared according to the TruSeq RNA Exome (Illumina) protocol. Library preparation workflow included purification and fragmentation of mRNA, first and second strand cDNA synthesis, end repair, 3´ends adenylation, adapters ligation, PCR amplification, library quantification, normalization and libraries pooling. Cleanup cycles are introduced between the mentioned steps.

Sequencing was performed on a NextSeq 550 / NovaSeq 600 Sequencer (Illumina). NextSeq 550 was performed with 75 bp 'paired-end' sequencing technology employing high-output flow cells. Calculations of RNA counts were performed as previously described[44,45].

Gene expression microarrays

A-673, TC-71, and SK-N-MC EwS cells containing either a Dox-inducible non-targeting control shRNA ('shCtr') or *EIF4EBP1*-targeting specific shRNAs (sh4E-BP1_1 or sh4E-BP1_2) were seeded in T25 flasks (TPP) and treated either with or without Dox (0.5 µg/ml; Sigma-Aldrich) for 96h. Thereafter, total RNA was extracted from one biological replicate for each condition with the Nucleospin II kit from Machery-Nagel and transcriptome profiled at IMGM laboratories (Martinsried, Germany). RNA quality was assessed with a Bioanalyzer and samples with RNA integrity numbers (RIN) > 9 were hybridized to Human Affymetrix Clariom D microarrays. Data were quantile normalized with Transcriptome Analysis Console (v4.0; Thermo Fisher Scientific) using the SST-RMA algorithm. Annotation of the data was performed using the Affymetrix library for Clariom D Array (version 2, human) at the gene level. Differentially expressed genes across shRNAs and cell lines were identified as follows: First, normalized gene expression signal was log2 transformed. To avoid false discovery artifacts due to the detection of only minimally expressed genes, we excluded all genes with a lower or just minimally higher gene expression signal than that observed for *ERG*, which is known to be virtually not expressed in *EWSR1::FLI1* positive EwS cell lines[7]. A mean log2FC was calculated for every cell line/construct and the mean log2FCs of both used specific shRNAs (sh_4E-BP1_1 and sh_4E-BP1_2) were summarized and normalized to that of the shCtr. Normalized log2FCs were summarized across cell lines. Genes showing a standard deviation of ≥0.5 between 3 cell lines were not considered for further analysis.

Analysis of published microarray gene expression data and patient survival analysis

Microarray data of 196 EwS tumors (Cohort 1) (GSE63157, GSE34620, GSE12102, GSE17618 and unpublished data[46–49]) for which well-curated clinical annotations were available were downloaded from the Gene Expression Omnibus (GEO). The data were either generated on Affymetrix HG-U133Plus2.0 or on Affymetrix HuEx-1.0-st microarray chips and were normalized separately by RMA using custom brainarray chip description files (CDF, v20) as previously described[50]. Batch effects were removed using ComBat[51]. Tumor purity was calculated using ESTIMATE[52] and only samples with a tumor purity >60% corresponding to The Cancer Genome Atlas (TCGA) standard (http://cancergenome.nih.gov/cancersselected/biospeccriteria) were kept for further analyses. Samples were stratified by their quartile intra-tumoral gene expression levels. Significance levels were calculated with a Mantel-Haenszel test (calculated using GraphPad Prism version 9). *P*-values <0.05 were considered as statistically significant.

Fast gene-set enrichment analysis (fGSEA) and single-sample GSEA (ssGSEA)

fGSEA was performed using the FGSEA R package (v 4.1.3) based on Gene Ontology (GO) biological processes terms from MSigDB (c5.all.v7.5.1 symbols.gmt, c2.all.v7.5.1 symbols.gmt) and GO terms were filtered for statistical significance (adjusted $P<0.05$) (10,000 permutations)[53,54]. Using the Affymetrix gene expression dataset comprising 196 EwS patients (Cohort 1), enrichment of gene sets that are among *EIF4EBP1* co-regulated genes were identified by ranking of Pearson´s correlation coefficient of the expression of each gene with *EIF4EBP1* expression and performance of a pre-ranked fGSEA.

Using the RNA-seq gene expression dataset comprising 99 primary EwS patients (Cohort 2), enrichment of gene sets that are among *EIF4EBP1* co-regulated genes and among chr8 regulated genes were identified by performing a pre-ranked fGSEA on a) ranked Pearson´s correlation coefficient between the expression of each gene with *EIF4EBP1* expression and on b) ranked mean log2FC as calculated for each gene between the group of EwS with and without chr8 gain.

Employing an integrated dataset inferred from MassSpec protein expression data and microarray gene expression data of A-673, SK-N-MC, and TC-71 EwS cell lines with/without 4E-BP1 knockdown containing differentially expressed proteins upon 4E-BP1 knockdown, all proteins were ranked by their mean log2 FC and a pre-ranked fGSEA was performed.

For inferring chr8 gene enrichment from gene expression data we applied single sample GSEA (ssGSEA)[55,56] on a EwS patient cohort of 196 tumor samples (Cohort 1) using gene sets from Ensembl 103 genes in cytogenetic band chr8 (Molecular Signatures Database (v7.4 MSigDB/c1.all.v7.5.symbols.gmt)). Genes considered for chr8 gene expression signature are listed in **Supplementary Table 9**. Based on the enrichment levels (ssGSEA scores) of chr8 we performed hierarchical clustering (pheatmap R package, version 1.0.12, https://cran.r-project.org/web/packages/pheatmap/pheatmap.pdf) to divide the EwS samples into a chr8 high and low gene expression group. To compare both groups regarding overall patient survival we performed a Kaplan Meier analysis. Significance levels were calculated with Mantel-Haenszel test (Graphpad Prism version 9).

Position Related Data Analysis (PREDA)

To validate appropriate clustering of Cohort 1 tumor samples into chr8 high and low gene expression groups we determined differentially expressed genes (DEGs) between both clusters using Limma[57] and Position Related Data Analysis (PREDA)[58] on iDEP[59] platform to map respective DEGs (FDR cut-off < 0.01) onto chromosomes. Using the Limma package[57], also DEGs of the mTOR signaling pathway were depicted.

Weighted gene correlation network analysis (WGCNA)

To construct a network, the WGCNA R package was used[53]. Briefly, a binary matrix of GO-/CCP-/CP-terms × genes (where 1 indicates the gene is present in the GO-/CCP-/CP-term and 0 indicates it is not) was created. Then, the Jaccard's distance for all possible pairs was computed to create a

symmetric GO/CCP/CP adjacent matrix. Clusters of similar GO-/CCP-/CP-terms were identified using dynamicTreeCut algorithm, and the top 20% highest edges were selected for visualization. The highest scoring node in each cluster was determined as the cluster label (rName). The obtained network and nodes files were fed into Cytoscape (v 3.8.0) for network design and visualization as previously described[60].

Histology

HE-staining of EwS xenografts was performed according to routine protocols. Mitoses of EwS xenografts were quantified in HE-stained slides by two blinded observers in 5 high-power fields per sample. Mitoses per sample were determined by mean of total 10 counted high-power fields across both observers. Necrosis of EwS xenografts were quantified in HE-stained slides by two blinded observers per sample (percentage of necrotic sample area). Necrosis per sample was determined by mean of quantified necrosis across both observers.

Statistics and software

Statistical data analysis was performed using GraphPad PRISM 9 (GraphPad Software Inc., CA, USA) on the raw data. If not otherwise specified in the figure legends comparison of two groups in functional *in vitro* experiments was carried out using a two-tailed Mann–Whitney test. If not otherwise specified in the figure legends, data are presented as dot plots with horizontal bars representing means, and whiskers representing the standard error of the mean (SEM). Sample size for all *in vitro* experiments were chosen empirically with at least 3 biological replicates. In Kaplan-Meier overall survival analyses, curves were calculated from all individual survival times of patients. Curves were compared by Mantel-Haenszel test to detect significant differences between the groups. For batch analyses of patient survival, the in-house custom code software GenEx was used, using the Mantel-Haenszel test for *P*-value calculation. Pearson´s correlation coefficients were calculated using Microsoft Excel or GraphPad PRISM 9 (GraphPad Software Inc., CA, USA). For *in vivo*

experiments, sample size was predetermined using power calculations with $\beta = 0.8$ and $\alpha = 0.05$ based on preliminary data and in compliance with the 3R system (replacement, reduction, refinement). Kaplan-Meier analyses of event-free survival (*in vivo* experiments) were carried out using GraphPad PRISM 9 (GraphPad Software Inc.). The definition of the type of events is given in the corresponding figure legends, but generally corresponds to humane experimental endpoints as defined above.

FUNDING

This project was mainly supported by a grant from the German Cancer Aid (DKH-70112257 to T.G.P.G.). The laboratory of T.G.P.G. is further supported by grants from the Matthias-Lackas foundation, the Dr. Leopold und Carmen Ellinger foundation, the Gert & Susanna Mayer foundation, the Deutsche Forschungsgemeinschaft (DFG 458891500), the German Cancer Aid (DKH-7011411, DKH-70114278), the Boehringer-Ingelheim foundation, the Dr. Rolf M. Schwiete foundation, the SMARCB1 association, the Ministry of Education and Research (BMBF; SMART-CARE and HEROES-AYA), and the Barbara and Wilfried Mohr foundation. J.M., I.O., M.S., A.B., were supported by the Ministry of Education and Research (HEROES-AYA). J.M. was additionally supported by the Heidelberg Foundation of Surgery and the Barbara und Wilfried Mohr foundation. J.L. was supported by a scholarship of the China Scholarship Council (CSC) and C.M.F. by a scholarship of the German Cancer Aid. The laboratory of J.A. was supported by grants from the Instituto de Salud Carlos III (PI20CIII/00020; DTS22CIII/00003; PMP21-00073), Fundación La Marató de TV3 (201937-30-31), Asociación Pablo Ugarte, Fundación Sonrisa de Alex, Asociación Todos somos Iván and Asociación Candela Riera.

ACKNOWLEGEMENTS

We thank Dr. Aruna Marchetto for her help in western blot assays. Support by the DKFZ Light Microscopy Facility is gratefully acknowledged.

AUTHOR CONTRIBUTIONS

C.M.F. performed most functional *in vitro* and *in vivo* experiments, analyzed the data, and designed the figures. M.F.O. performed functional experiments, helped in shRNA design and lentiviral transduction of cell lines. K.A. performed MassSpec and analyzed MassSpec data. A.E. performed bioinformatic analyses. J.L. helped in conduction of *in vivo* experiments. T.L.B.H., M.M.L.K., E.V. assisted in experimental procedures. R.W. performed cloning of vectors. F.W. performed analyses of histology. F.Z. assisted in experimental procedures. S.O., R.I., A.B. helped in performance of *in vivo* experiments. J.A., A.S., W.H., U.D. provided clinical information. M.S. provided financial support and laboratory infrastructure. O.W., I.O. performed drug screens that are still ongoing. S.M.P., G.L. provided biological and technical guidance. L.R.-P. conducted methylation arrays and performed bioinformatic analyses. J.K. provided financial support and laboratory infrastructure for performance of MassSpec. F.-C.A. carried out functional *in vitro* and *in vivo* experiments. J.M. coordinated and supervised the study, provided biological and technical guidance, performed functional experiments as well as bioinformatic and histological analyses, analyzed and interpreted all data, wrote the paper, and provided financial support. T.G.P.G designed, coordinated, and supervised the study, provided biological and technical guidance, analyzed and interpreted all data, wrote the paper and provided financial support and laboratory infrastructure. All authors read and approved the final manuscript.

CONFLICT OF INTEREST

We declare no conflicts of interest.

REFERENCES

1. Grünewald, T. G. P. *et al.* Ewing sarcoma. *Nat. Rev. Dis. Primer* **4**, 5 (2018).
2. Grünewald, T. G. P. *et al.* Chimeric EWSR1-FLI1 regulates the Ewing sarcoma susceptibility gene EGR2 via a GGAA microsatellite. *Nat. Genet.* **47**, 1073–1078 (2015).
3. Musa, J. *et al.* Cooperation of cancer drivers with regulatory germline variants shapes clinical outcomes. *Nat. Commun.* **10**, 4128 (2019).
4. Machiela, M. J. *et al.* Genome-wide association study identifies multiple new loci associated with

Ewing sarcoma susceptibility. *Nat. Commun.* **9**, 3184 (2018).
5. Tirode, F. *et al.* Genomic landscape of Ewing sarcoma defines an aggressive subtype with co-association of STAG2 and TP53 mutations. *Cancer Discov.* **4**, 1342–1353 (2014).
6. Brohl, A. S. *et al.* The genomic landscape of the Ewing Sarcoma family of tumors reveals recurrent STAG2 mutation. *PLoS Genet.* **10**, e1004475 (2014).
7. Crompton, B. D. *et al.* The genomic landscape of pediatric Ewing sarcoma. *Cancer Discov.* **4**, 1326–1341 (2014).
8. Mugneret, F., Lizard, S., Aurias, A. & Turc-Carel, C. Chromosomes in Ewing's sarcoma. II. Nonrandom additional changes, trisomy 8 and der(16)t(1;16). *Cancer Genet. Cytogenet.* **32**, 239–245 (1988).
9. Maurici, D. *et al.* Frequency and implications of chromosome 8 and 12 gains in Ewing sarcoma. *Cancer Genet. Cytogenet.* **100**, 106–110 (1998).
10. Armengol, G. *et al.* Recurrent gains of 1q, 8 and 12 in the Ewing family of tumours by comparative genomic hybridization. *Br. J. Cancer* **75**, 1403–1409 (1997).
11. Nacev, B. A. *et al.* Clinical sequencing of soft tissue and bone sarcomas delineates diverse genomic landscapes and potential therapeutic targets. *Nat. Commun.* **13**, 3405 (2022).
12. Su, X. A. *et al.* RAD21 is a driver of chromosome 8 gain in Ewing sarcoma to mitigate replication stress. *Genes Dev.* **35**, 556–572 (2021).
13. Tarkkanen, M. *et al.* Clinical correlations of genetic changes by comparative genomic hybridization in Ewing sarcoma and related tumors. *Cancer Genet. Cytogenet.* **114**, 35–41 (1999).
14. Hattinger, C. M. *et al.* Prognostic impact of chromosomal aberrations in Ewing tumours. *Br. J. Cancer* **86**, 1763–1769 (2002).
15. Orth, M. F. *et al.* Systematic multi-omics cell line profiling uncovers principles of Ewing sarcoma fusion oncogene-mediated gene regulation. *Cell Rep.* **41**, 111761 (2022).
16. Mackintosh, C. *et al.* 1q gain and CDT2 overexpression underlie an aggressive and highly proliferative form of Ewing sarcoma. *Oncogene* **31**, 1287–1298 (2012).
17. Kullendorff, C. M. *et al.* Cytogenetic aberrations in Ewing sarcoma: are secondary changes associated with clinical outcome? *Med. Pediatr. Oncol.* **32**, 79–83 (1999).
18. Musa, J. *et al.* Eukaryotic initiation factor 4E-binding protein 1 (4E-BP1): a master regulator of mRNA translation involved in tumorigenesis. *Oncogene* (2016) doi:10.1038/onc.2015.515.
19. Saxton, R. A. & Sabatini, D. M. mTOR Signaling in Growth, Metabolism, and Disease. *Cell* **168**, 960–976 (2017).
20. Goss, K. L. *et al.* The translational repressor 4E-BP1 regulates RRM2 levels and functions as a tumor suppressor in Ewing sarcoma tumors. *Oncogene* **40**, 564–577 (2021).
21. Garraway, L. A., Verweij, J. & Ballman, K. V. Precision oncology: an overview. *J. Clin. Oncol. Off. J. Am. Soc. Clin. Oncol.* **31**, 1803–1805 (2013).
22. Musa, J. & Grünewald, T. G. P. Interaction between somatic mutations and germline variants contributes to clinical heterogeneity in cancer. *Mol. Cell. Oncol.* **7**, 1682924 (2020).
23. Jahromi, M. S., Jones, K. B. & Schiffman, J. D. Copy Number Alterations and Methylation in Ewing's Sarcoma. *Sarcoma* **2011**, 362173 (2011).
24. Brisset, S. *et al.* CGH analysis of secondary genetic changes in Ewing tumors: correlation with metastatic disease in a series of 43 cases. *Cancer Genet. Cytogenet.* **130**, 57–61 (2001).
25. Ferreira, B. I. *et al.* Array CGH and gene-expression profiling reveals distinct genomic instability patterns associated with DNA repair and cell-cycle checkpoint pathways in Ewing's sarcoma. *Oncogene* **27**, 2084–2090 (2008).
26. Ozaki, T. *et al.* Genetic imbalances revealed by comparative genomic hybridization in Ewing tumors. *Genes. Chromosomes Cancer* **32**, 164–171 (2001).
27. Selvarajah, S. *et al.* Characterization of trisomy 8 in pediatric undifferentiated sarcomas using advanced molecular cytogenetic techniques. *Cancer Genet. Cytogenet.* **174**, 35–41 (2007).
28. Wolman, S. R., Gundacker, H., Appelbaum, F. R., Slovak, M. L., & Southwest Oncology Group. Impact of trisomy 8 (+8) on clinical presentation, treatment response, and survival in acute myeloid leukemia: a Southwest Oncology Group study. *Blood* **100**, 29–35 (2002).

29. Wang, W. *et al.* Impact of trisomy 8 on treatment response and survival of patients with chronic myelogenous leukemia in the era of tyrosine kinase inhibitors. *Leukemia* **29**, 2263–2266 (2015).
30. Wang, W. *et al.* Clinical significance of trisomy 8 that emerges during therapy in chronic myeloid leukemia. *Blood Cancer J.* **6**, e490 (2016).
31. Sreekantaiah, C., Karakousis, C. P., Leong, S. P. & Sandberg, A. A. Trisomy 8 as a nonrandom secondary change in myxoid liposarcoma. *Cancer Genet. Cytogenet.* **51**, 195–205 (1991).
32. Mrózek, K., Karakousis, C. P., Perez-Mesa, C. & Bloomfield, C. D. Translocation t(12;22)(q13;q12.2-12.3) in a clear cell sarcoma of tendons and aponeuroses. *Genes. Chromosomes Cancer* **6**, 249–252 (1993).
33. Wu, S. & Wagner, G. Deep computational analysis details dysregulation of eukaryotic translation initiation complex eIF4F in human cancers. *Cell Syst.* **12**, 907-923.e6 (2021).
34. Hauffe, L. *et al.* Eukaryotic translation initiation factor 4E binding protein 1 (EIF4EBP1) expression in glioblastoma is driven by ETS1- and MYBL2-dependent transcriptional activation. *Cell Death Discov.* **8**, 91 (2022).
35. Levy, T. *et al.* 4EBP1/2 support tumorigenicity and cell survival during energetic stress by translationally regulating fatty acid synthesis. 2022.09.09.507243 Preprint at https://doi.org/10.1101/2022.09.09.507243 (2022).
36. Livak, K. J. & Schmittgen, T. D. Analysis of relative gene expression data using real-time quantitative PCR and the 2(-Delta Delta C(T)) Method. *Methods San Diego Calif* **25**, 402–408 (2001).
37. Wiederschain, D. *et al.* Single-vector inducible lentiviral RNAi system for oncology target validation. *Cell Cycle Georget. Tex* **8**, 498–504 (2009).
38. Marchetto, A. & Romero-Pérez, L. Western Blot Analysis in Ewing Sarcoma. *Methods Mol. Biol. Clifton NJ* **2226**, 15–25 (2021).
39. Funk, C. M. & Musa, J. Proliferation Assessment by Trypan Blue Exclusion in Ewing Sarcoma. *Methods Mol. Biol. Clifton NJ* **2226**, 151–158 (2021).
40. Schindelin, J. *et al.* Fiji: an open-source platform for biological-image analysis. *Nat. Methods* **9**, 676–682 (2012).
41. Schneider, C. A., Rasband, W. S. & Eliceiri, K. W. NIH Image to ImageJ: 25 years of image analysis. *Nat. Methods* **9**, 671–675 (2012).
42. Cidre-Aranaz, F. & Ohmura, S. Tumor Growth Analysis of Ewing Sarcoma Cell Lines Using Subcutaneous Xenografts in Mice. *Methods Mol. Biol. Clifton NJ* **2226**, 191–199 (2021).
43. Koelsche, C. *et al.* Sarcoma classification by DNA methylation profiling. *Nat. Commun.* **12**, 498 (2021).
44. Stichel, D. *et al.* Routine RNA sequencing of formalin-fixed paraffin-embedded specimens in neuropathology diagnostics identifies diagnostically and therapeutically relevant gene fusions. *Acta Neuropathol. (Berl.)* **138**, 827–835 (2019).
45. McPherson, A. *et al.* deFuse: an algorithm for gene fusion discovery in tumor RNA-Seq data. *PLoS Comput. Biol.* **7**, e1001138 (2011).
46. Savola, S. *et al.* High Expression of Complement Component 5 (C5) at Tumor Site Associates with Superior Survival in Ewing's Sarcoma Family of Tumour Patients. *ISRN Oncol.* **2011**, 168712 (2011).
47. Postel-Vinay, S. *et al.* Common variants near TARDBP and EGR2 are associated with susceptibility to Ewing sarcoma. *Nat. Genet.* **44**, 323–327 (2012).
48. Scotlandi, K. *et al.* Overcoming resistance to conventional drugs in Ewing sarcoma and identification of molecular predictors of outcome. *J. Clin. Oncol. Off. J. Am. Soc. Clin. Oncol.* **27**, 2209–2216 (2009).
49. Volchenboum, S. L. *et al.* Gene Expression Profiling of Ewing Sarcoma Tumors Reveals the Prognostic Importance of Tumor-Stromal Interactions: A Report from the Children's Oncology Group. *J. Pathol. Clin. Res.* **1**, 83–94 (2015).
50. Sannino, G. *et al.* Gene expression and immunohistochemical analyses identify SOX2 as major risk factor for overall survival and relapse in Ewing sarcoma patients. *EBioMedicine* **47**, 156–162

(2019).
51. Johnson, W. E., Li, C. & Rabinovic, A. Adjusting batch effects in microarray expression data using empirical Bayes methods. *Biostat. Oxf. Engl.* **8**, 118–127 (2007).
52. Yoshihara, K. *et al.* Inferring tumour purity and stromal and immune cell admixture from expression data. *Nat. Commun.* **4**, 2612 (2013).
53. Korotkevich, G. *et al.* Fast gene set enrichment analysis. 060012 Preprint at https://doi.org/10.1101/060012 (2021).
54. Subramanian, A. *et al.* Gene set enrichment analysis: a knowledge-based approach for interpreting genome-wide expression profiles. *Proc. Natl. Acad. Sci. U. S. A.* **102**, 15545–15550 (2005).
55. Hänzelmann, S., Castelo, R. & Guinney, J. GSVA: gene set variation analysis for microarray and RNA-seq data. *BMC Bioinformatics* **14**, 7 (2013).
56. Barbie, D. A. *et al.* Systematic RNA interference reveals that oncogenic KRAS-driven cancers require TBK1. *Nature* **462**, 108–112 (2009).
57. Ritchie, M. E. *et al.* limma powers differential expression analyses for RNA-sequencing and microarray studies. *Nucleic Acids Res.* **43**, e47 (2015).
58. Ferrari, F., Solari, A., Battaglia, C. & Bicciato, S. PREDA: an R-package to identify regional variations in genomic data. *Bioinforma. Oxf. Engl.* **27**, 2446–2447 (2011).
59. Ge, S. X., Son, E. W. & Yao, R. iDEP: an integrated web application for differential expression and pathway analysis of RNA-Seq data. *BMC Bioinformatics* **19**, 534 (2018).
60. Waszak, S. M. *et al.* Germline Elongator mutations in Sonic Hedgehog medulloblastoma. *Nature* **580**, 396–401 (2020).

FIGURES

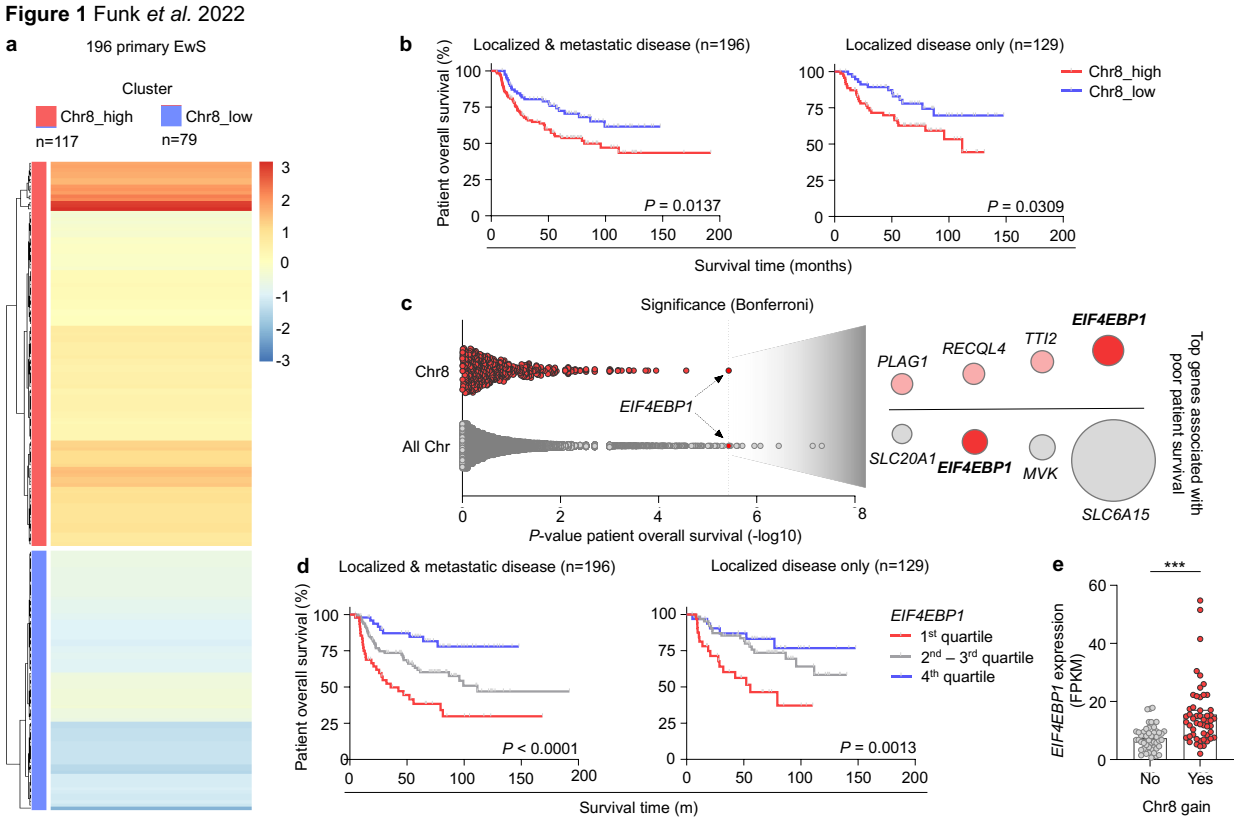

Figure 1: Chromosome 8 gain drives overexpression of the clinically relevant translation initiation factor 4E-BP1 in EwS. a Heat map showing 196 EwS patient tumors (Cohort 1) according to an inferred chr8 gene expression signature as assessed by single-sample Gene Set Enrichment Analysis (ssGSEA) followed by hierarchical clustering assigning each sample into either a high or low chr8 signature expression group. **b** Kaplan-Meier overall survival analysis of 196 EwS patients (Cohort 1) stratified into either a high or low chr8 signature expression group as described in (a). Kaplan-Meier plots are shown separately either for patients with localized & metastatic disease (n=196, left) or exclusively for patients with localized disease (n=129, right). *P*-value determined by Mantel-Haenszel test. **c** Kaplan-Meier overall survival batch analysis as assessed for every gene covered in transcriptomic profiling of 196 EwS patients (Cohort 1). Chr8-located genes were additionally depicted separately. The dashed line indicates the Bonferroni-adjusted *P*-value threshold for significance. The dots represent other genes reaching top statistical significance for association with poor overall patient survival after Bonferroni correction next to *EIF4EBP1*. **d** Kaplan-Meier overall survival analysis of 196 EwS patients (Cohort 1) stratified by quartile *EIF4EBP1* expression. Kaplan-Meier plots are shown separately either for patients with localized & metastatic disease (n=196, left) or exclusively patients with localized disease (n=129, right). *P*-value determined by Mantel-Haenszel test. **e** *EIF4EBP1* expression as measured by RNA-seq in 99 primary EwS (Cohort 2) depending on the presence of chromosome 8 gain as determined by methylation array. *P*-value determined by two-tailed Mann-Whitney test, horizontal bars represent means and whiskers represent the SEM. ***$P < 0.001$.

Figure 2 Funk *et al.* 2022

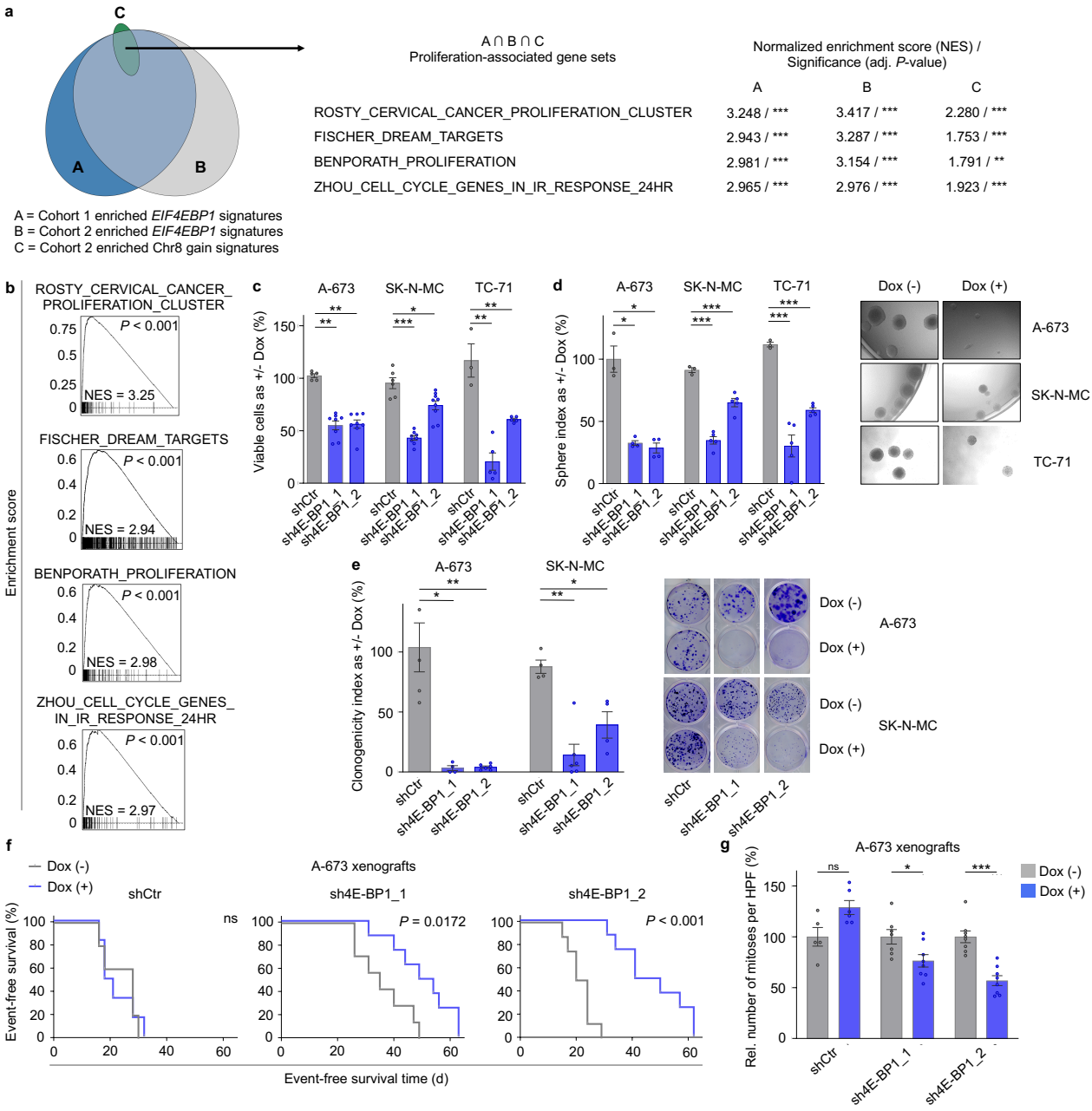

Figure 2: High 4E-BP1 expression promotes EwS growth *in vitro* and *in vivo*. a Area-proportional Venn diagram of gene sets enriched with *EIF4EBP1* expression in cohort 1 (A) and 2 (B) as well as with chr8 gain in cohort 2 (C) as determined by fGSEA. Exemplary gene sets representing a proliferation-associated enrichment signature in the overlap between A, B, and C were shown with respective normalized enrichment scores (NES) and significance levels. **b** fGSEA enrichment plots of exemplary gene sets given in (a). **c** Relative viable cell count of A-673, SK-N-MC, and TC-71 cells containing either Dox-inducible specific shRNA constructs directed against *EIF4EBP1* (sh4E-BP1_1 or sh4E-BP1_2) or a non-targeting shControl (shCtr). Cells were grown either with or without Dox for 96h. Horizontal bars represent means, and whiskers represent the SEM, n ≥ 4 biologically independent experiments. **d** Sphere formation in A-673, SK-N-MC, and TC-71 cells containing shRNA constructs directed against *EIF4EBP1* (sh4E-BP1_1 or sh4E-BP1_2) or a non-targeting shControl (shCtr) treated with or without Dox for 8–14 d. Horizontal bars represent means, and whiskers represent the SEM, n ≥ 3 biologically independent experiments. Two-tailed unpaired t-test with Welch´s correction. Representative images of spheres are shown on the right. **e** Relative colony number of A-673 and SK-N-MC cells containing either Dox-inducible

specific shRNA constructs directed against *EIF4EBP1* (sh4E-BP1_1 or sh4E-BP1_2) or a non-targeting shControl (shCtr). Cells were grown either with or without Dox for 8–14 d. Horizontal bars represent means, and whiskers the SEM, $n \geq 4$ biologically independent experiments. Representative images of colony formation are shown on the right. **f** Kaplan-Meier analysis of event-free survival of NSG mice xenografted with A-673 cells containing either Dox-inducible specific shRNA constructs directed against *EIF4EBP1* (sh4E-BP1_1 or sh4E-BP1_2) or a non-targeting shControl (shCtr). Once tumors were palpable, mice were randomized and treated with either vehicle (–) or Dox (+), $n \geq 5$ animals per condition. An 'event' is recorded when tumors reached a size maximum of 15 mm in one dimension. *P*-values determined via Mantel-Haenszel test. **g** Quantification of mitoses in HE-stained slides of xenografts described in (f). Five high-power fields (HPF) were counted per sample. Horizontal bars represent means, and whiskers represent the SEM, $n \geq 4$ samples per condition. ***$P < 0.001$, **$P < 0.01$, *$P < 0.05$, ns = not significant; *P*-values determined via two-tailed Mann-Whitney test if not otherwise specified.

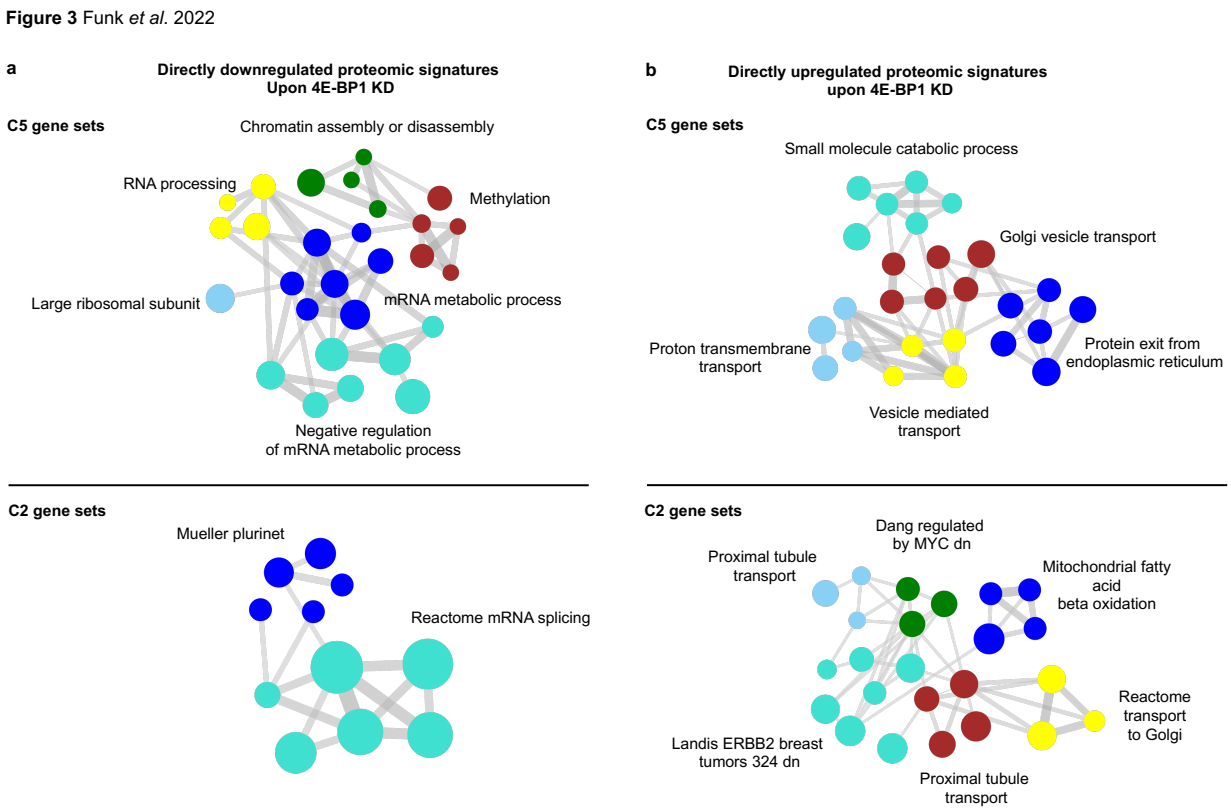

Figure 3: 4E-BP1 directly guides a multifunctional proteomic network. a Weighted Gene Correlation Network Analysis (WGCNA) depicting directly downregulated functional proteomic signatures upon 4E-BP1 knockdown considering C5 (upper) and C2 (lower) collections of gene sets of the Molecular Signatures Database (MSigDB). Network depicts signatures presenting *P*-values < 0.05 and a normalized enrichment score (NES) > 2. **b** WGCNA depicting directly upregulated functional proteomic signatures upon 4E-BP1 knockdown considering C5 (upper) and C2 (lower) collections of gene sets of the MSigDB. Network depicts signatures presenting *P*-values < 0.05 and an NES > 2.

Supplementary Figure 1 Funk *et al.* 2022

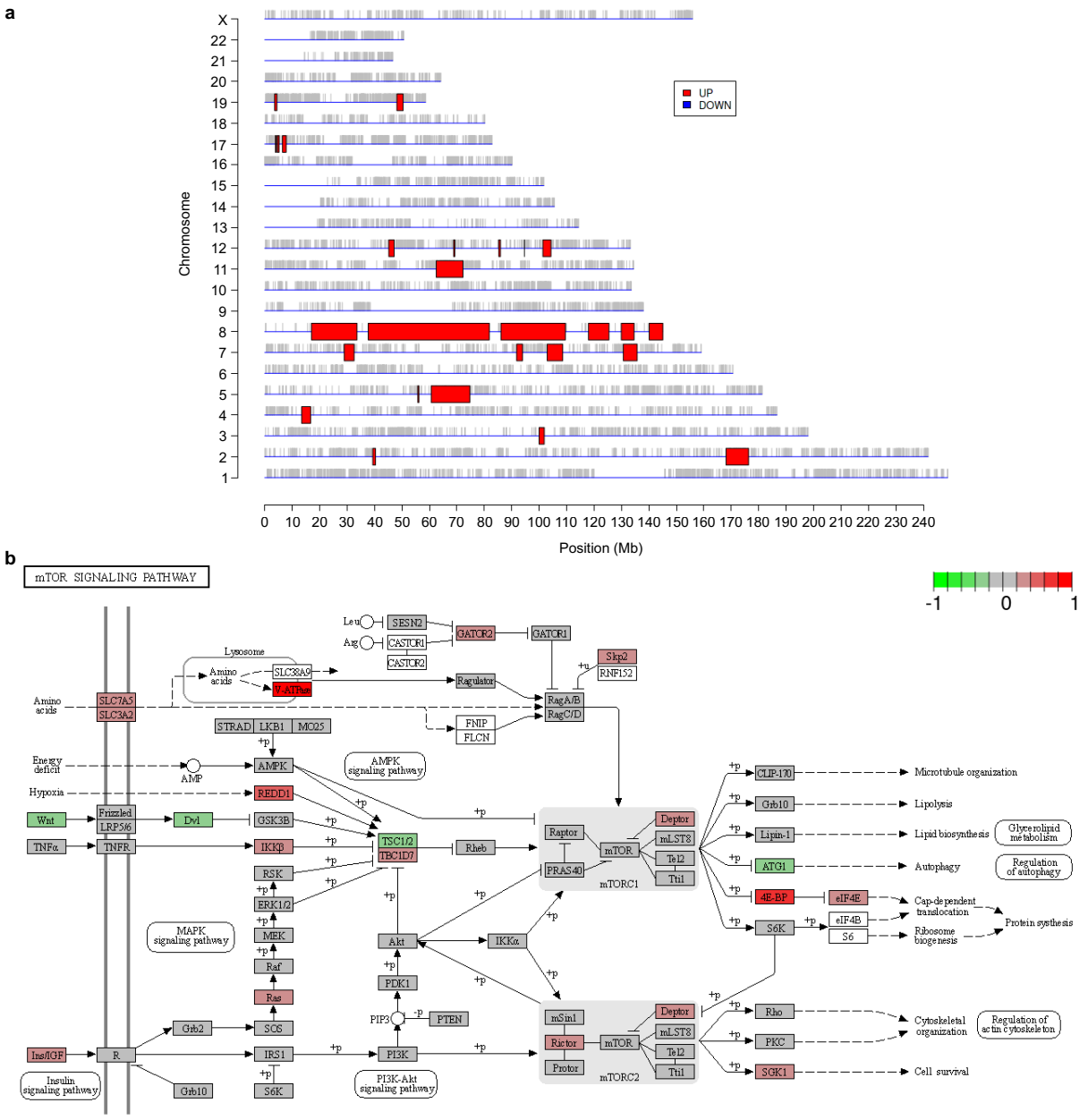

Supplementary Figure 1: Chromosomal location and mTOR pathway representation of genes differentially upregulated in the chr8 high gene expression signature group in EwS.
a Differentially expressed genes (DEGs) between chr8 high and low gene expression cluster mapped onto chromosomes using Position Related Data Analysis (PREDA). **b** DEGs between chr8 high and low gene expression within the mTOR signaling pathway.

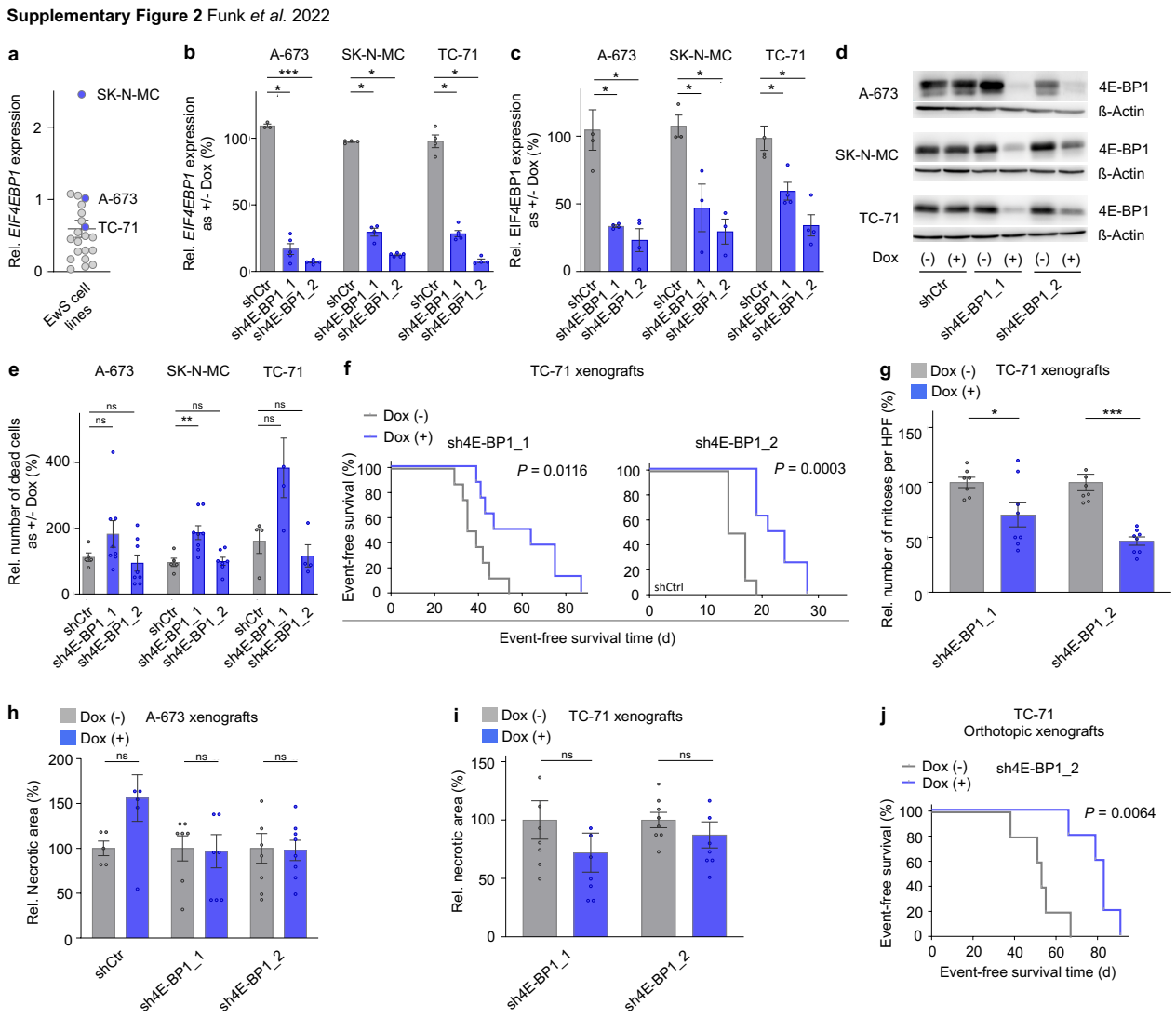

Supplementary Figure 2: RNAi-mediated knockdown of 4E-BP1 inhibits EwS growth.
a Relative *EIF4EBP1* expression in 21 wild-type EwS cell lines as determined by qRT-PCR. **b** Relative *EIF4EBP1* expression as assessed by qRT-PCR in A-673, SK-N-MC, and TC-71 cells containing either Dox-inducible specific shRNA constructs directed against *EIF4EBP1* (sh4E-BP1_1 or sh4E-BP1_2) or a non-targeting shControl (shCtr). Cells were grown either with or without Dox for 96h. Horizontal bars represent means, and whiskers represent the SEM, n ≥ 3 biologically independent experiments. **c** Relative 4E-BP1 expression as assessed by quantified western blotting in A-673, SK-N-MC, and TC-71 cells containing either Dox-inducible specific shRNA constructs directed against *EIF4EBP1* (sh4E-BP1_1 or sh4E-BP1_2) or a non-targeting shControl (shCtr). Cells were grown either with or without Dox for 96h. *P*-values determined via one-tailed Mantel-Haenszel test. **d** Representative western blots as described in (b) are shown. ß-actin served as a loading control. **e** Relative number of dead cells as assessed by Trypan blue exclusion in A-673, SK-N-MC, and TC-71 cells containing either Dox-inducible specific shRNA constructs directed against *EIF4EBP1* (sh4E-BP1_1 or sh4E-BP1_2) or a non-targeting shControl (shCtr). Cells were grown either with or without Dox for 96h. Horizontal bars represent means, and whiskers represent the SEM, n ≥ 4 biologically independent experiments. **f** Kaplan-Meier analysis of event-free survival of NSG mice xenografted with TC-71 cells containing Dox-inducible specific shRNA constructs directed against *EIF4EBP1* (sh4E-BP1_1 or sh4E-BP1_2). Once tumors were palpable, mice were randomized and treated with either vehicle (–) or Dox (+), n =8 animals per condition. An 'event' is recorded when tumors reached a size maximum of 15 mm in one dimension.

P-values determined via Mantel-Haenszel test. **g** Quantification of mitoses in HE-stained slides of xenografts described in (f). Five high-power fields (HPF) were counted per sample. Horizontal bars represent means, and whiskers represent the SEM, $n \geq 7$ samples per condition. **h** Quantification of necrotic area on HE-stained slides of A-673 xenografts described in (f). Five high-power fields (HPF) were analyzed per sample. Horizontal bars represent means, and whiskers represent the SEM, $n \geq 5$ samples per condition. **i** Quantification of necrotic area on HE-stained slides of TC-71 xenografts described in (f). Five high-power fields (HPF) were analyzed per sample. Horizontal bars represent means, and whiskers represent the SEM, $n \geq 7$ samples per condition. **j** Kaplan-Meier analysis of event-free survival of NSG mice orthotopically xenografted into the proximal tibia with TC-71 containing a Dox-inducible specific shRNA construct directed against *EIF4EBP1* (sh4E-BP1_2). One day after injection of the cells, mice were randomized and treated with either vehicle (–) or Dox (+), n =5 animals per condition. An 'event' is recorded when the mice exhibited signs of limping at the injected leg. *P*-values determined via Mantel-Haenszel test. ***$P < 0.001$, **$P < 0.01$, *$P < 0.05$, ns = not significant; *P* values determined via two-tailed Mann-Whitney test if not otherwise specified.

Supplementary Figure 3 Funk *et al.* 2022

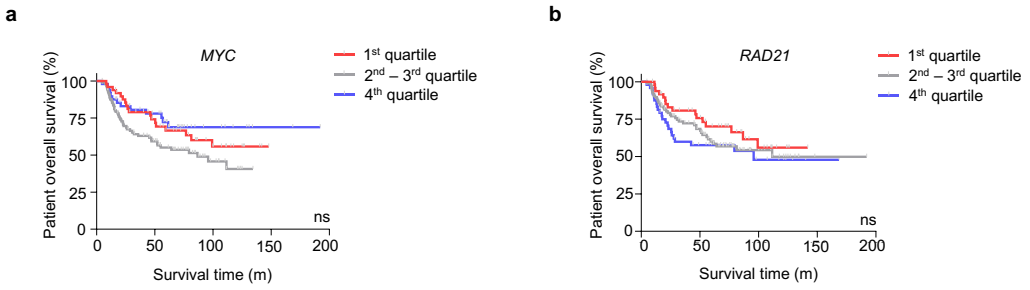

Supplementary Figure 3: Kaplan-Maier survival analysis in Cohort 1 stratifying patients by quartile *MYC* and *RAD21* expression. a Kaplan-Meier overall survival analysis of 196 EwS patients (Cohort 1) stratified by quartile *MYC* expression. **b** Kaplan-Meier overall survival analysis of 196 EwS patients (Cohort 1) stratified by quartile *RAD21* expression. *P*-values determined by Mantel-Haenszel test. ns = not significant.